JMEPEG (2025) 34:13247–13258
https://doi.org/10.1007/s11665-024-10119-z

1059-9495/$19.00

ORIGINAL RESEARCH ARTICLE

Investigation of Weldability in Friction Stir Welding of Aluminum Alloys AA5754 and AA2024

Suleyman Kilic, Fahrettin Ozturk, and Mehmet Fatih Demirdogen

Submitted: 29 September 2023 / Revised: 19 April 2024 / Accepted: 28 June 2024 / Published online: 24 September 2024

This study examined the weldability of AA5754 and AA2024 aluminum alloys using the friction stir welding (FSW). Through systematic analysis of welding parameters such as rotational and traverse speeds, we have identified configurations to improve the mechanical properties and efficiency of the welds significantly. The optimal parameters, specifically a rotational speed of 1200 rpm combined with a traverse speed of 45 mm/min, were found to yield the best outcomes. The welding efficiency achieved was 54% for the AA5754 alloy and 26% for the AA2024 alloy, with a combined alloy efficiency of 47% when welding dissimilar materials. The study has conclusively demonstrated that appropriate parameter selection is crucial for maximizing weld strength and minimizing defects such as voids and cracks. This research contributes to the understanding of the FSW applicability in joining dissimilar aluminum alloys, emphasizing the importance of parameter optimization to achieve desirable mechanical characteristics and weld integrity.

Keywords AA5754 welding, AA2024 welding, friction stir welding, FSW, weldability, welding of dissimilar materials

1. Introduction

Welding technologies play a crucial role in material joining processes in various industries. Recently, numerous research studies have been conducted on welding technologies specifically focusing on developing new methods for joining materials that are either not easily weldable or pose challenges with traditional welding methods. Friction stir welding (FSW) has emerged as one of the widely adopted techniques in this context. The FSW is a solid-state joining method used to join metals and alloys (Ref 1). The FSW, a mature solid-state welding technique, involves temperature, mechanics, metallurgy and interactions, has become a revolutionary welding technique because of its energy efficiency, environmental friendliness, and high-quality joints (Ref 2). The state-of-the-art friction based welding techniques are characterized by low peak temperature, severe plastic deformation, energy efficiency and nonpollution, which can simultaneously realize the mechanical and chemical bonding, improving mechanical performances (Ref 3). In particular, the weldability of certain aluminum alloys using the FSW has been extensively investigated. Aluminum alloys are commonly used in many industries due to their lightweight and high strength. Therefore, research on the effective weldability and post-welding mechanical properties of aluminum alloys holds significant importance. The FSW has found applications in various industries such as automotive, aerospace, and shipbuilding (Ref 4-9). It is employed in the assembly of lightweight structures, like aluminum structures in vehicles, production of aircraft fuselage panels, and construction of marine structures (Ref 10-15).

The FSW is based on the principle of generating frictional heat through a rotating tool and mixing the material using a pin located at the tool's tip to create a weld joint. The tool design and process parameters, such as rotational speed and traverse speed, have a significant impact on welding efficiency. The material flow was affected by the temperature and the profile of tool. The design of tool can be considered for avoiding weld thinning. Elimination of weld thinning was reported in Ref (16, 17). Researches reveal that how flash defects were eliminated and weld thinning was avoided. For eliminating of root kissing bond, the root-enhanced FSW, with an enlarged-tip pin and concave structure, was a good choice to enhance the root tolerance in thick plates (Ref 18). Most of the studies in the literature focus on determining and optimizing these parameters. Process parameters such as dwell time of the tool on the material surface, tool rotation, traverse speed, axial force, plunge depth, and tool tilt angle affect the welding quality (Ref 19-23). It is well known that optimization of these parameters has great effect on the joint strength properties (Ref 24, 25). Material placement arrangement is also an important factor when dissimilar materials are welded in the FSW. Placing the softer material in the direction of tool rotation can result in better weld quality (Ref 26). The microstructure of the base material plays a crucial role in determining weldability (Ref 27). The presence of significant defects such as voids, lack of fusion, and tunnel formation can affect the mechanical properties of the weld joint (Ref 28-31). These defects can occur due to inappropriate process parameters, inadequate tool design, or material compatibility factors (Ref 32). According to experimental results, an increase in rotational speed leads to

Suleyman Kilic, Department of Mechanical Engineering, Faculty of Engineering and Architecture, Kırşehir Ahi Evran University, Kırşehir, Türkiye; **Fahrettin Ozturk**, Department of Mechanical Engineering, Faculty of Engineering and Natural Sciences, Ankara Yıldırım Beyazıt University, Ankara, Türkiye; and Turkish Aerospace Industries, Inc., Ankara, Türkiye; and and **Mehmet Fatih Demirdogen**, Uygurlar Makina, Organized Industrial Zone, Kırşehir, Türkiye. Contact e-mail: suleymankilic@gmail.com.

Table 1 Chemical composition of the materials (Weight %)

Materials	Fe	Si	Cu	Cr	Mn	Mg	Zn	Zi + Ti	Al
2024	0.5	0.5	3.8-4.9	0.1	0.3–0.9	1.2–1.8	0.25	0.15	Balance
5754	0.4	0.4	0.1	0.3	0.5	2.6–3.6	0.2	0.15	Balance

Table 2 Chemical composition of AISI H13 hot work tool steel (Ref 41)

Alloy	C	Cr	Mo	V
Weight (%)	0.40	5.30	1.40	1.00

tunnel defects (Ref 33). An increase in welding speed, on the other hand, causes larger wormhole defects to form (Ref 34).

A welding efficiency of 65% was achieved when welding AA5754 alloy by the FSW (Ref 35). Fernandes et al. (Ref 36) investigated the effect of cooling on the friction stir weld quality in AA2024-T351 alloy. They showed that cooling with a cold air jet did not have a significant effect on weld quality or grain refinement. Mehta (Ref 37) investigated the modified friction stir clinching (MFSC) process in AA5754-O and AA2024-T3 alloys. They emphasized that material positioning significantly influenced the bonding characteristics and grain formation behavior. Kumar et al. (Ref 38) examined the friction stir welding parameters for 2024 aluminum alloy using a tool with a tapered cylindrical pin profile. They highlighted the effect of parameters such as tool rotational speed on welding quality. It was stated that larger tunnel defects occurred at higher traverse speeds and tool rotational speeds. Hu et al. (Ref 39) studied the microstructure and mechanical properties of 5 mm thick AA2024-O alloy using an FSW welding machine, followed by plastic deformation and subsequent heat treatment. They demonstrated that the tensile and yield strengths of the friction stir weld were significantly increased after plastic deformation due to grain refinement. However, they emphasized that the strength of the friction stir weld decreased significantly due to grain growth during subsequent heat treatment. Memon et al. (Ref 40) examined the effects of positioning and tool rotational speed using the modified friction stir clinching method on AA5754-O and AA2024-T3 plates. They stated that material positioning had an effect on the mechanical properties. The fact that the hard material is in the upper position provides a higher peak temperature. Regardless of the weld type, the hard material on top causes a higher dislocation density. For this reason, it is recommended to place the harder Al alloy on top of the soft alloy.

The purpose of this study is to investigate the weldability of aluminum alloys AA5754 and AA2024 using the FSW in both similar and dissimilar configurations. A tapered threaded tool was specifically manufactured, and the welding process was conducted on a CNC vertical machining center. The research focuses on examining the impact of rotational and traverse speeds on the mechanical properties of the joints. The experimental determination of the tensile and three-point bending strengths of both welded and unwelded specimens underlines the practical applications of this research. Uniquely, this study advances the current state of the art by demonstrating how optimized welding parameters can significantly enhance joint quality and performance, providing valuable insights for industrial applications of the FSW in aluminum alloys.

2. Materials and Methods

In this research, both 2.5 mm thick AA2024-T3 and AA5754-H111 alloys were joined by the FSW in similar and dissimilar combinations. The changes in the mechanical properties of the base materials and the welded materials were investigated through tensile and three-point bending tests. The chemical compositions of the materials in this study is given in Table 1. AISI H13 hot work tool steel was used as the tool material. The chemical composition of the tool material is provided in Table 2 below (Ref 41).

In order to perform the FSW process, a clamping plate was first produced from St52 steel material with a thickness of 20 mm. The design of the plate took into consideration the efficient execution of the welding process and the ease of attaching and detaching the specimens. The plate, which was cut using laser technology, underwent surface and edge scanning on a CNC vertical machining center to ensure flatness. A 2 mm channel was created in the center of the plate to allow the specimens to align axially and to prevent any slippage in the welding direction (Fig. 1a). The final state of the plate after the machining process is shown in Fig. 1b. After the machining process, during the preparation of the experimental setup, the alignment of the channel wall axis with the plate edge wall axes was confirmed to be parallel by checking them with a comparator. Once the welding table and specimens were attached to the plate, the alignment of both the plate axis and the specimen axes was checked using a comparator. Since the tool had to progress along the line where the two materials joined, each component's axis was individually checked before each operation to ensure the correct position of the probe with respect to the workpiece. This ensured that the welding tool advanced along the junction line of the plates. Fig. 1c illustrates the assembled state of the welding table and the plates to be welded, while Fig.1d demonstrates the verification of flatness.

The schematic view of the produced tapered threaded tool is shown in Fig. 2. The tool features a tapered pin with a tip diameter of 4 mm, a base with a diameter of 6 mm, and a pin height of 2.3 mm. A right-hand tapered thread with a 1 mm pitch was formed on its surface. Most curial aspects of the tool in the FSW are its design, material, and hardness. The H13 steel used in this study had a pre-hardening hardness of 14.8 HRC. After necessary machining operations, it underwent a hardening process to achieve a hardness value of 55 HRC. The process parameters chosen were 1200/45, 1600/60, and 2000/75 for the rotational speed/traverse speed ratio. The tool rotation direction was determined as clockwise. The orientation of the welding materials was parallel to the rolling direction. The arrangement

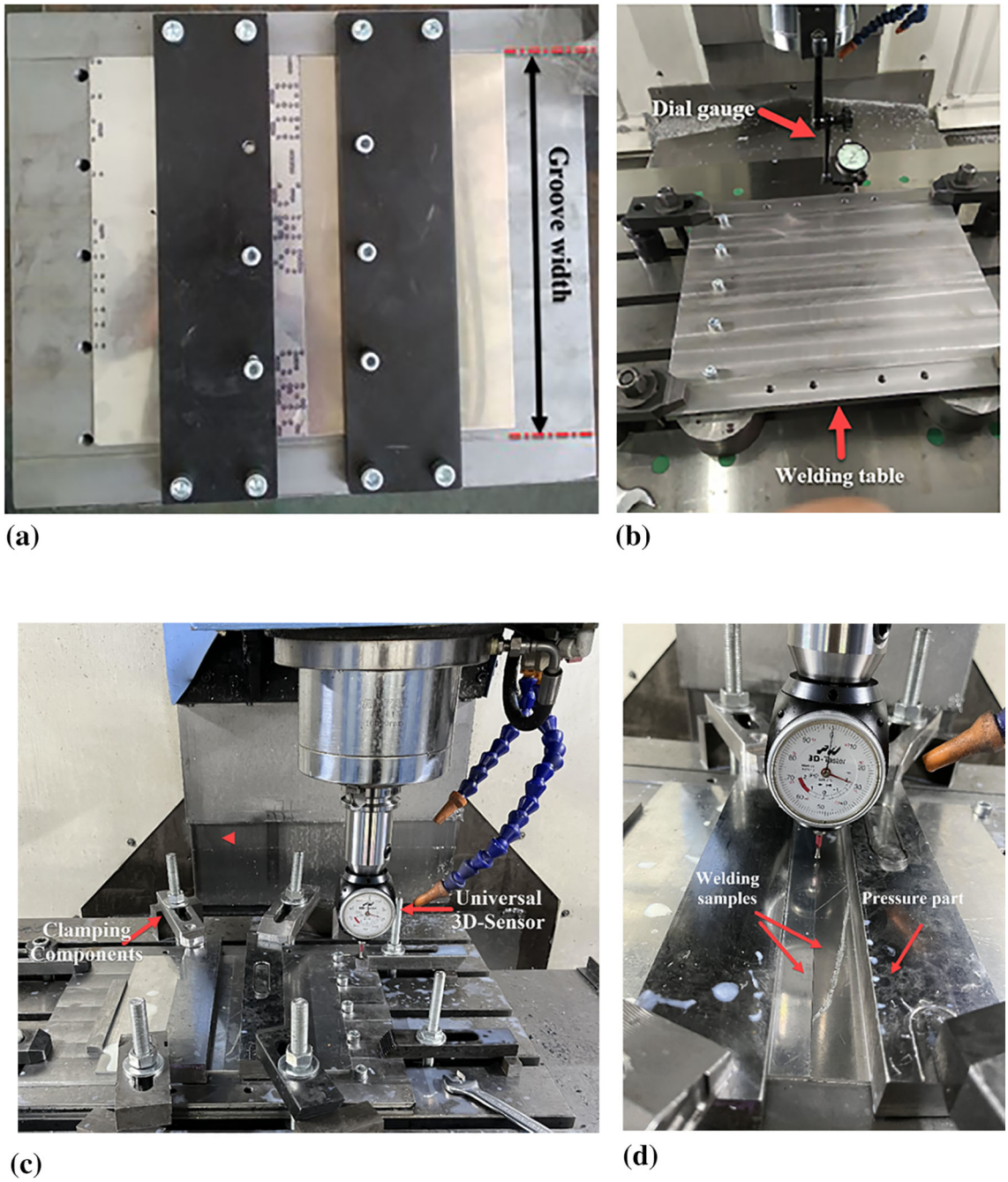

Fig. 1 (a) 2 mm channel in the table, (b) Producing of the welding table, (c) Attachment of the welding table and specimens, (d) Verification of flatness

of the materials and the process parameters are provided in Table 3. Since the position affects the mechanical properties (Ref 42), AA2024 was placed on the advancing side due to its higher mechanical strength. For dissimilar metals in the FSW, the harder materials usually was placed at the advancing side for higher heat generation to thermo-plasticize, and better fluidity materials at the retreating side (Ref 43).

The tool design and process schematic used in this study are shown in Fig. 3. This process consists of two steps. In the first step, the tool shoulder is brought into contact with the material surface, and frictional heat is expected to be generated for approximately 12 seconds. In the second step, the tool is advanced along the weld line at the predetermined rotational speed and traverse amount.

The welded specimens were cut in ambient air on a laser machine to the dimensions shown in Fig.4, following the ASTM-E8 standard. The preparation of the specimens from the welding plate was conducted in accordance with the ISO 25239-4 standard. Tensile tests were conducted on the specimens at room temperature (RT) using a Shimadzu Autograph 100 kN universal testing machine at a crosshead speed of 1 mm/min. Unit deformation measurements were taken using a video-type extensometer. Each test was repeated at least three times.

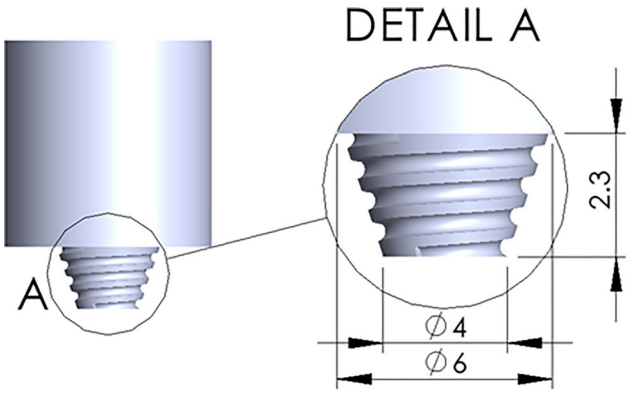

Fig. 2 Dimensions of the tapered threaded tool produced schematically

The welded specimens were subjected to three-point bending tests using a bending punch with a 5 mm radius. The specimens were prepared with dimensions of 210 × 20 × 2.5 mm, as shown in Fig. 5. The bending tests were conducted using a Jinan Victory brand bending test machine with a capacity of 100 kN.

The center point of the punch was positioned on the welding upper surface, aligned with the center of the welding zone. The platform supports were adjusted to have a center distance of 130 mm. The support points had a 5 mm radius. The punch applied bending force to the specimen by making contact with the welding upper surface. The bending speed was set at 10 mm/min. A detailed illustration of the bending test setup is shown in Fig. 6.

Table 3 Welding materials and process parameters

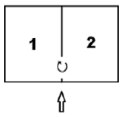	Process parameters		
	Rotational speed (rpm) - Traverse speed (mm/min)	**Rotational speed (rpm) - Traverse speed (mm/min)**	**Rotational speed (rpm) - Traverse speed (mm/min)**
2024-2024	1200-45	1600-60	2000-75
2024-5754	1200-45	1600-60	2000-75
5754-5754	1200-45	1600-60	2000-75

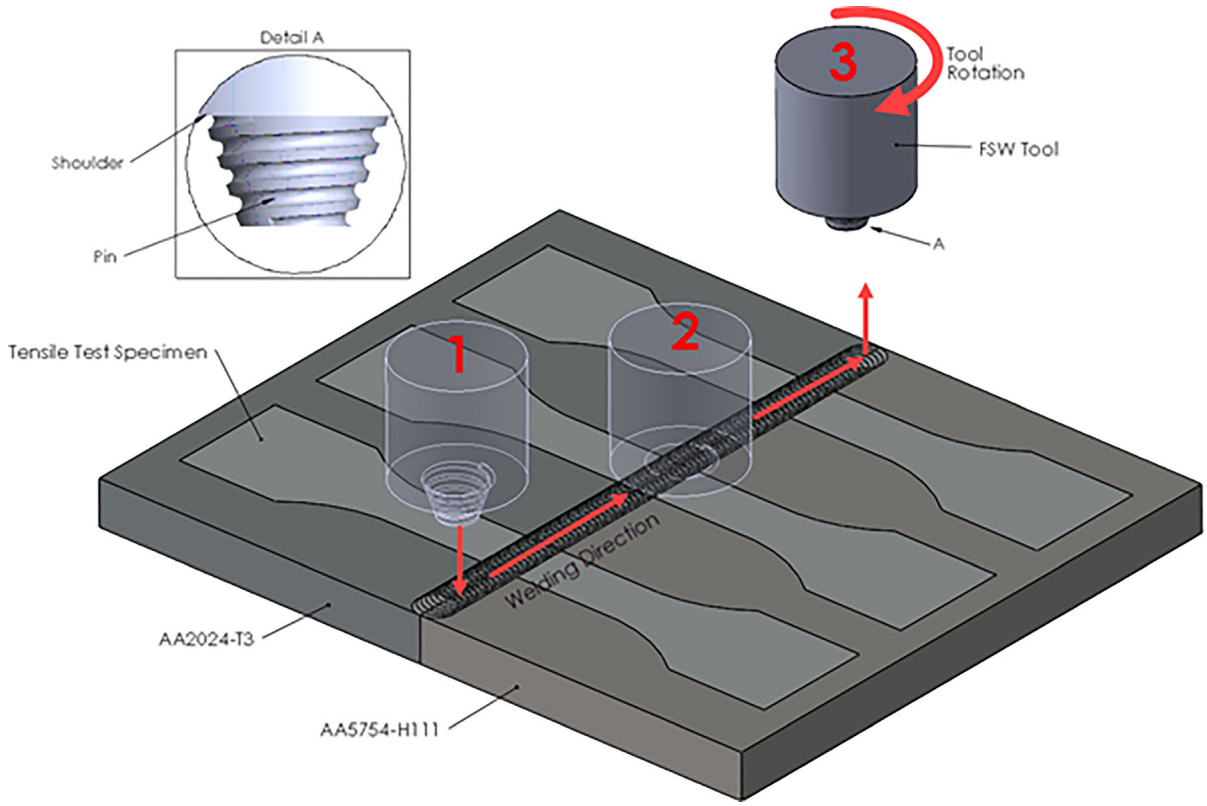

Fig. 3 Schematic representation of the FSW process

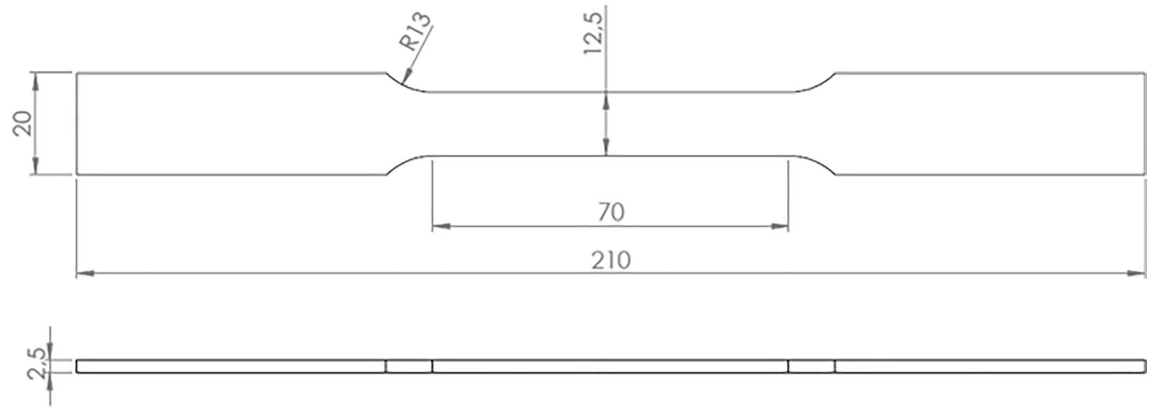

Fig. 4 Dimensions of the tensile test specimen

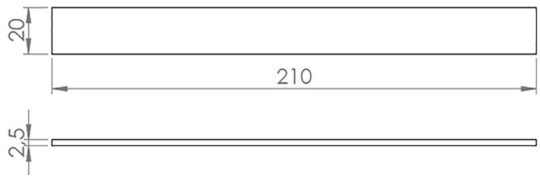

Fig. 5 Dimensions of the bending test specimen

3. Result and Discussion

The 5754-H111 and 2024-T3 aluminum alloys were welded together in dissimilar combinations and with different materials using various rotational speeds and traverse speeds as shown in Table 3. The welding tool plunged to a depth of 2.3 mm, resulting in 9 welded specimens. An image of the welding process is shown in Fig. 7a. No deformation was observed in the tool as a result of the welding process. However, due to inappropriate process parameters, a small amount of aluminum material was observed to smear onto the threaded region on the pin of the tapered tool, as shown in Fig. 7b.

During the experimental studies, a trial was conducted to examine the effect of traverse speed on surface quality. In this trial, 2024-T3 and 5754-H111 aluminum alloys were joined by the FSW process at a rotational speed of 2000 rpm and traverse speeds of 30, 50, and 80 mm/min. As the traverse speed increased, as seen in Fig. 8, the surface quality of the weld seam deteriorated, and void formation was observed in the weld seam. Increasing the traverse speeds causes less heat accumulation in the weld, and lower ductility. Similar observations have been seen in the literature. Patel et al. (Ref 44) emphasized the significance of welding speed, tool rotation speed, and tool geometry on welding quality. Additionally, Iqbal et al. (Ref 45) stated in their research that the temperature on the left side of the welding traverse line was higher than the right side, highlighting the influence of plunge depth as well. The deterioration in surface quality is attributed not only to the use of inappropriate process parameters but also to the lack of suitable parameters for the tool. Variations in temperature and material flow in different regions of the weld seam result in a poorer surface on the advancing side of the weld seam. Furthermore, improper application of plunge depth led to insufficient chip removal and accumulation around the weld seam area. The key point here is to thoroughly understand the effects of parameters and optimize them accordingly (Table 4).

Both welded and un-welded specimens were tested at a tensile speed of 1 mm/min. In all specimens, whether welded or un-welded, brittle fracture was observed. Fig. 9 presents the stress-strain curve of the un-welded AA2024-T3 alloy and the AA5754-H111 alloy.

To examine the effect of strain rate, AA5754-AA5754 two plates were welded by the FSW at a rotational speed of 2000 rpm and a traverse speed of 75 mm/min. Tensile specimens were obtained from this welded plate and tested at two different speeds (1 mm/min and 5 mm/min). As shown in Fig. 10, increasing the strain rate resulted in a slight decrease in strength.

In the FSW of different materials, the positioning of the material was examined. AA5754 and AA2024 plates to be welded were attached to the welding table with two different orientations, right and left of the tool's advancing direction, and they were welded under the same tool rotation and travel speeds, and the process was completed with the tool rotating in a clockwise direction. As shown in Fig. 11, the positioning of the material is an important parameter. The strength increased when the AA2024 alloy was positioned on the advancing side. This can be attributed to the clockwise rotation of the tool, which carries the high-strength AA2024 material from the left to the right, resulting in a more durable weld. Verma et al. (Ref 46) found temperature differences between the advancing side and the retreating side in their study. It is believed that this difference, along with the change in material positioning, leads to differences in mechanical properties. Ma et al. (Ref 47) emphasized that the mechanical properties in the weld zone are dependent on the welding tool as well as the process parameters and material flow.

The effect of traverse speed on the FSW of different materials was investigated. AA2024-AA5754 alloy pairs were welded with a rotational speed of 1600 rpm, while varying the traverse speeds at 60 mm/min and 80 mm/min, with the tool rotating clockwise. As shown in Fig. 12, higher strength and ductility were achieved at a traverse speed of 80 mm/min. Li et al. (Ref 48) conducted a study where they observed an initial increase in weld strength with increasing traverse speed, reaching an optimum point, and then a decrease with further increase in traverse speed. Wen et al. (Ref 49), who examined the effect of traverse speed on tensile strength and elongation in the FSW with a coil tool, observed an increase in both tensile

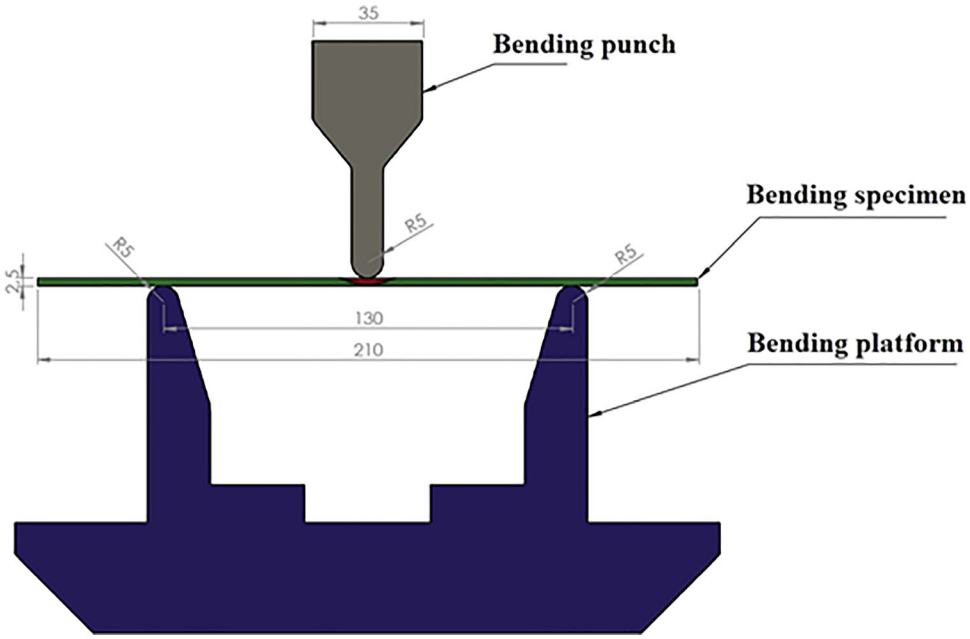

Fig. 6 Schematic representation of the bending test setup

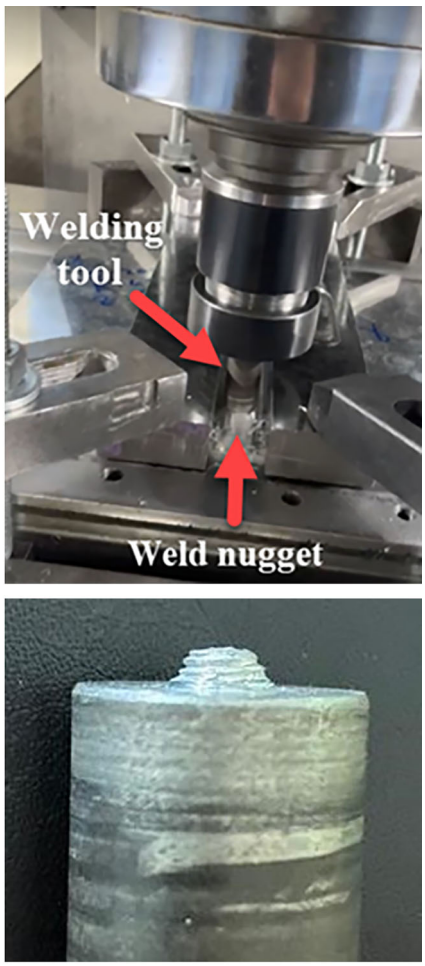

Fig. 7 (a) Performance of the welding process, (b) Picture of the tool after the process was performed

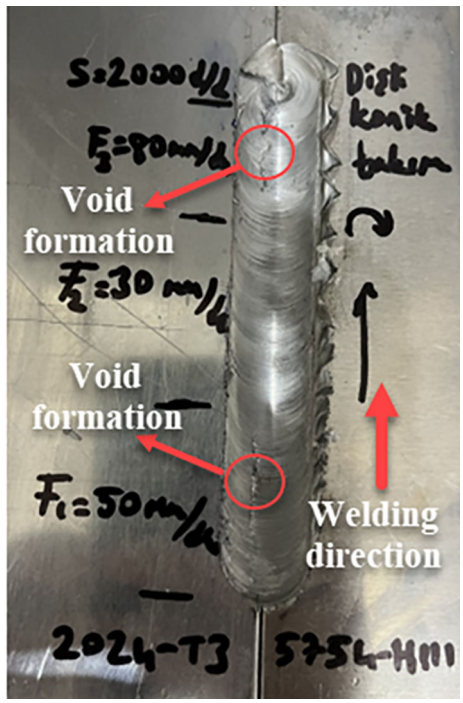

Fig. 8 Effect of welding speed on the surface quality

strength and elongation up to a certain value with increasing traverse speed.

The AA2024-AA5754 materials were welded by the FSW by using different parameters. As shown in Fig. 13, the highest strength and ductility value were achieved at 1200 rpm rotation speed and 45 mm/min traverse speed. It has been noted in previous studies that the weld strength can vary due to differences in welding parameters. Temperature variations have been highlighted as factors that can affect the grain size in the

Table 4 Findings from the literature and experimental results

Material pair	Material thickness (mm)	Welding tensile strength (MPa)	Base material tensile strength (MPa)	Process Parameters (rpm/min-mm/min)	Efficiency (%)	Tool geometry	References
6061-T6	0.5	220.3	310	1500/500	71.06	Triflat	(Ref 58)
5052-H32	6	208.9	228	700/65	91.62	Square conical	(Ref 59)
5052	3	205.0	214	1200/30	95.79	Conical	(Ref 60)
5754-H111	2	223.4	240	1500/30	93.08	Conical	(Ref 61)
5086-H34	6	264.5	324	1250/80	81.64	Square	(Ref 54)
2024-T4/7075-T6	4/5	378.7	446/572 (Med:509)	1200/50	74.40	Threaded conical	(Ref 20)
5754-H114/soft steel	2	222.3	240,93/440 (Med:340.465)	750/30	65.29	Cylindrical	(Ref 62)
2024-T3/5754-H111	2.5	172.0	485/240 (Med:362.5)	1200/45	47.44	Conical	This study
5754-H111	2.5	130.0	240	1200/45	54.17	Conical	This study
2024-T3	2.5	128.0	485	1200/45	26.39	Conical	This study
2024	…	204.2	306.5		66.62	TIG welding	(Ref 63)
5754	…	183.0	237.1		77.18	TIG welding	(Ref 63, 64)

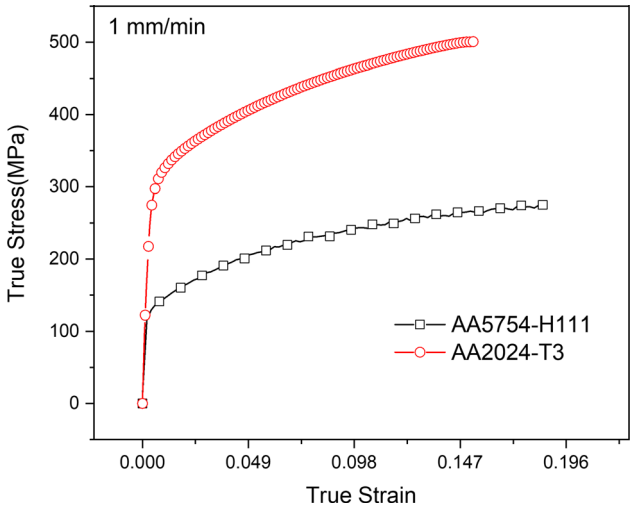

Fig. 9 Tensile strength graph of specimens taken from the base materials

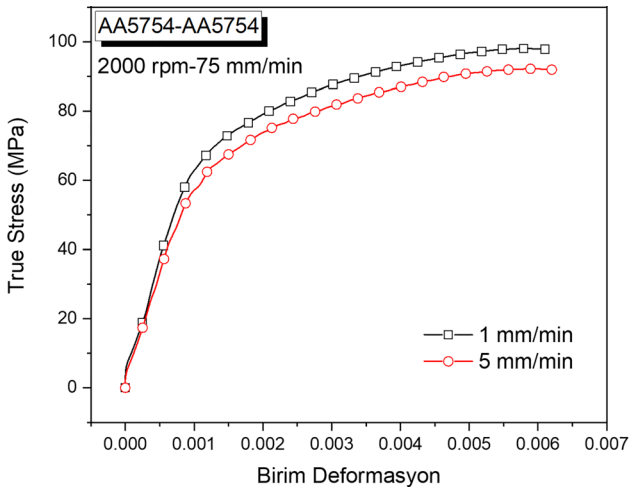

Fig. 10 Stress-strain curve of welded AA5754 alloy at different strain rates

microstructure (Ref 44, 45, 50, 51). Different welding parameters have resulted in higher strength and ductility in the weld seam.

When AA5754-AA5754 materials were joined by the FSW at different parameters, it was observed that the rotation speed and traverse speed remained important factors. As seen in Fig. 14, the highest strength and ductility values were obtained at 1200 rpm and 45 mm/min traverse speed. In other parameter combinations, ductility, and strength decrease. A similar study conducted on this alloy achieved better strength values at lower rotation speeds (450–900 rpm) using different tools (Ref 52).

When AA2024-AA2024 materials are welded by the FSW, the rotation speed and traverse speed were also important factors. As seen in Fig. 15, the material experiences fracture shortly after the onset of plastic deformation. The highest strength values were achieved at the parameters of 1200 rpm - 45 mm/min and 2000 rpm - 75 mm/min traverse speed. It has been observed that the heat-affected zone of the welded region undergoes grain growth, leading to an increase in hardness (Ref 53, 54). In addition to welding defects, the hardness increases in the materials results in welded specimens exhibiting lower ductility compared to the un-welded materials, leading to faster failure.

According to the results of the research, it was observed that that the highest fracture strength values belong to the AA2024 - AA5754 plate pair. The highest fracture strength value was obtained in the weld seam produced with a tool rotation speed of 1200 rpm and a traverse speed of 45 mm/min (Fig. 16). Mahany et al. (Ref 20) achieved the maximum strength in the

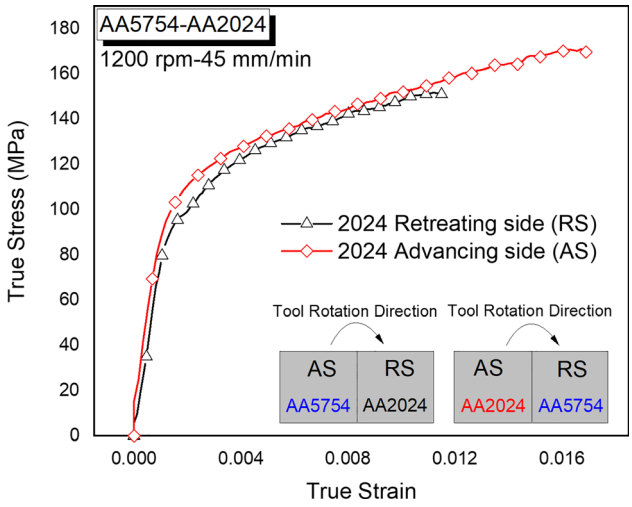

Fig. 11 The effect of positioning on the weld strength

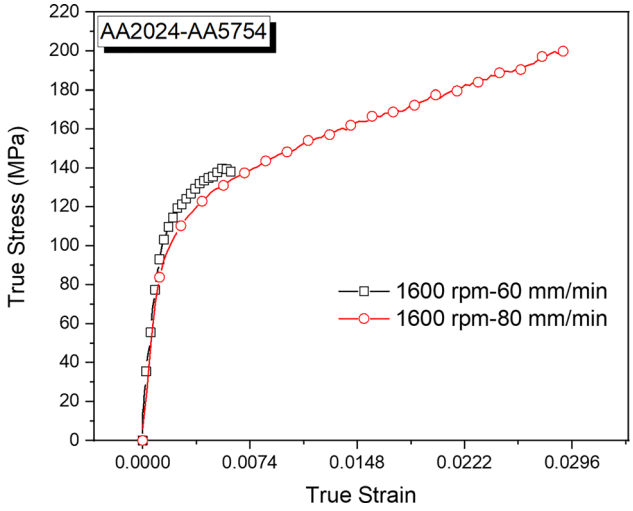

Fig. 12 The effect of traverse speed on weld strength

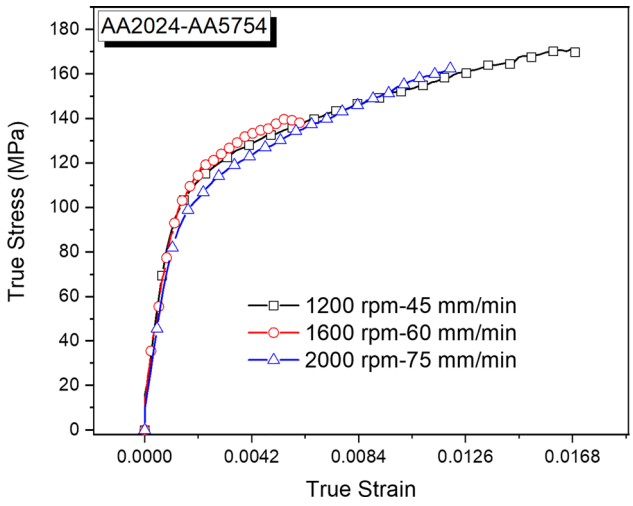

Fig. 13 Tensile strength graph of the AA2024-AA5754 weld specimen

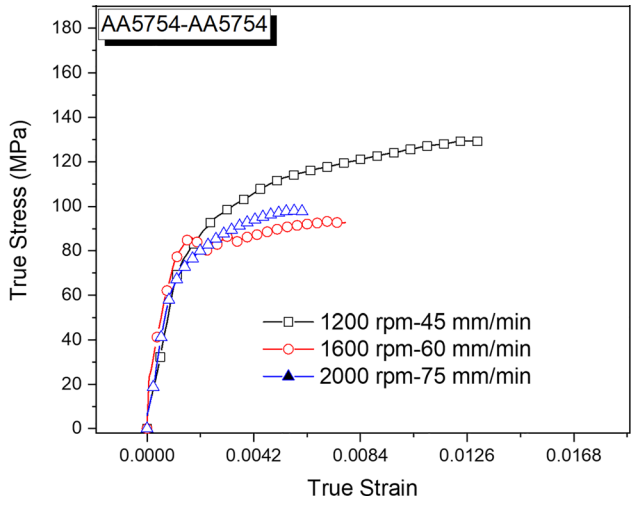

Fig. 14 Tensile strength graph of the AA5754-AA5754 welded sample

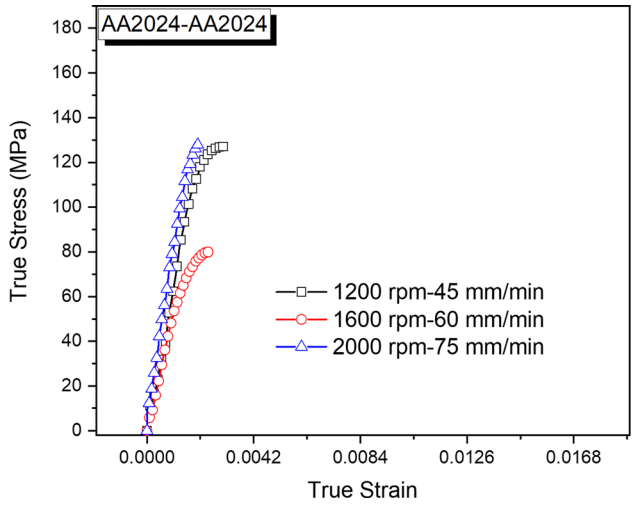

Fig. 15 Tensile strength graph of the AA2024-2024 welded specimen

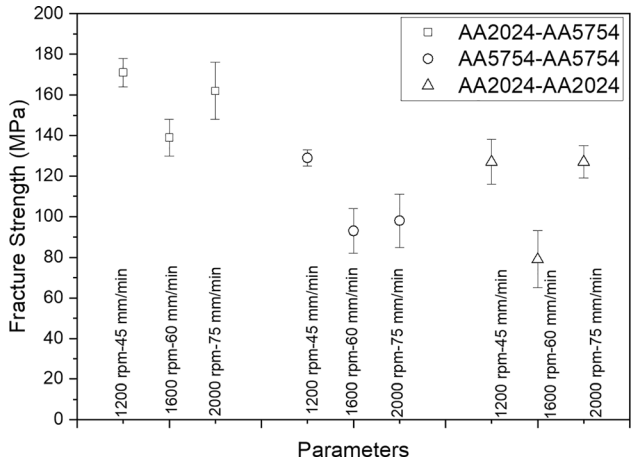

Fig. 16 Variation of fracture strength under different welding parameters

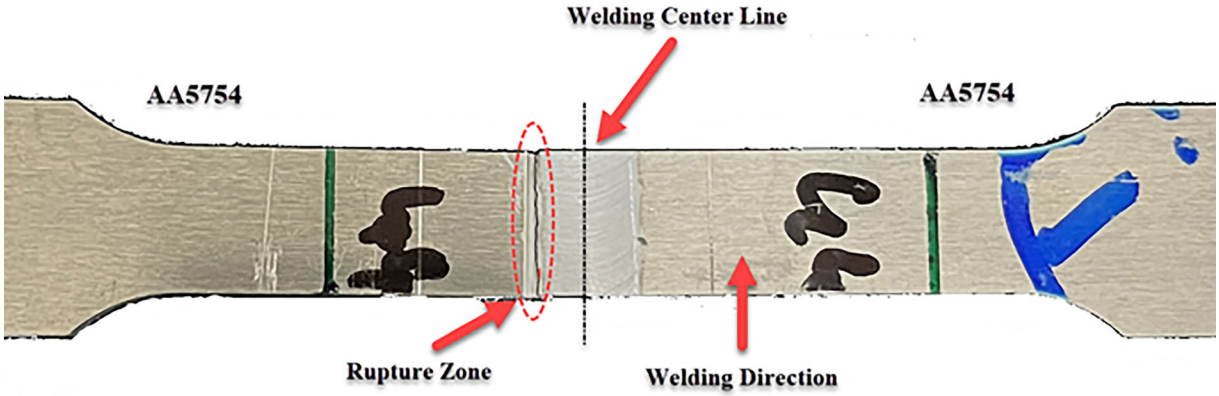

Fig. 17 Fracture region of AA5754 specimens under tensile testing

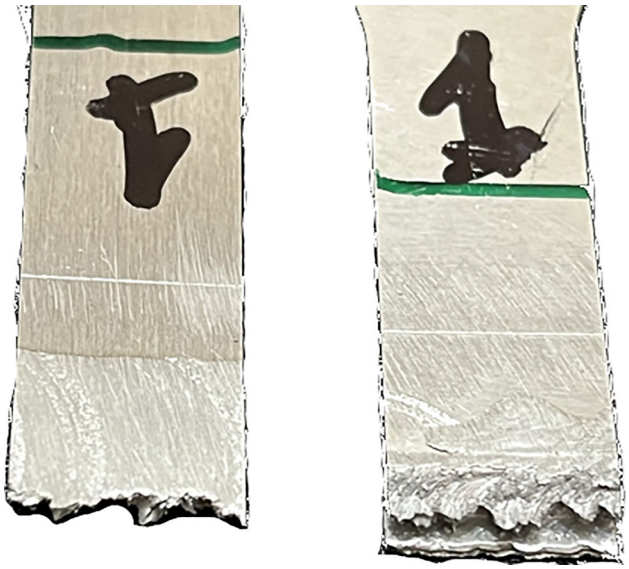

Fig. 18 Fracture region of a specimen after tensile testing

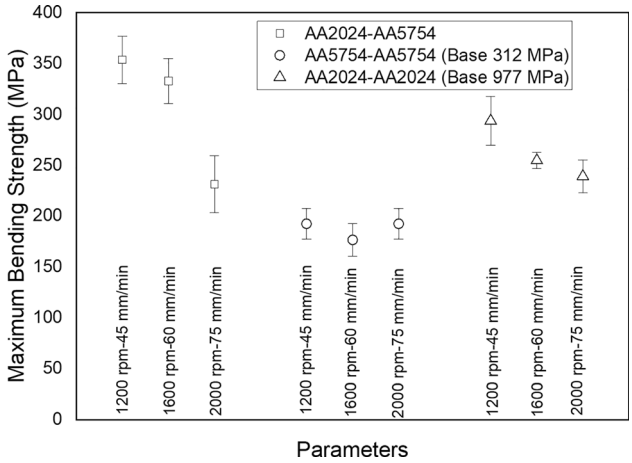

Fig. 19 Results of the three-point bending test

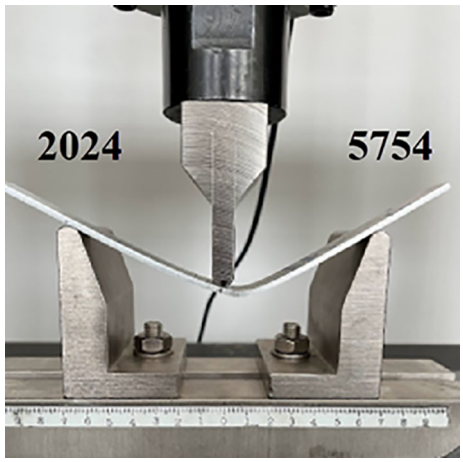

Fig. 20 Bending test image of the AA2024-5754 welded sample

FSW experiments on 2024-T4 material at a tool rotation speed of 1200 rpm.

When the specimen obtained from the joining of two AA5754 alloy plates was subjected to tensile testing, the fracture mechanism was observed to develop from the advancing side of the weld line, and the crack propagated towards the center, leading to fracture, as shown in Fig. 17. This fracture mechanism is also present in welds made with the same material and different material types.

After conducting tensile tests, it was observed that the microstructure of a different specimen was not homogeneous. In addition, voids were observed in the upper and lower regions of the material, namely the weld upper surface and lower surface, where the integrity of the weld was not maintained. These voids, caused by the presence of small cracks resulting from the notch effect due to the deformation of the material, lead to fracture. The visual representation of the fracture region is shown in Fig. 18. Kumar et al. (Ref 55) demonstrated the influence of tool geometry on the mixing efficiency. Therefore, when designing the tool geometry, it is necessary to consider the ability to generate sufficient heat for homogeneous mixing of the material. Türkyılmaz et al. (Ref 56) also conducted a study on investigating the most efficient tool geometry. The study emphasized the importance of both homogeneous mixing and the generation of sufficient heat.

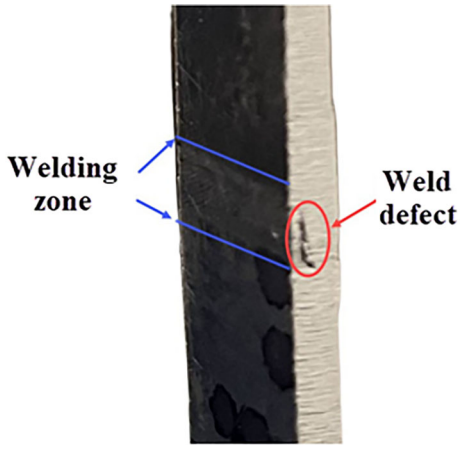

Fig. 21 Welding defect in the AA2024-T3 alloy

The results of the bending tests are shown in Fig. 19. Upon examining the graph, it can be observed that the bending strengths confirm the findings of the tensile tests conducted on the welded samples. The highest bending strength was achieved with the processing parameters of 1200 rpm and 45 mm/min.

When a bending force of 10 mm/min was applied to the sample of AA5754 - AA2024 alloys joined by the FSW, it was observed that the sample bent towards the AA5754 alloy, which has a lower yield strength compared to the other alloy (Fig. 20). This indicates that the weld seam, being a combination of the two materials, is stronger than the AA5754 alloy with lower yield strength. Msomi et al. (Ref 57), who subjected AA1050-H14 and AA5083-H111 materials joined by the FSW to a three-point bending test, it was found that bending occurred towards the AA1050-H14 material with lower yield strength. Similar results were obtained in this study.

In Fig. 21, a welding defect occurring in the internal region of AA2024 alloy was observed. Although there are no visible issues on the welding surface, the presence of voids within the internal sections has resulted in lower strength values for these materials. Therefore, in the FSW, which has a complex process structure, it is necessary to determine the most suitable parameters. It is likely for such errors to occur when the materials are not completely filled. Optimal process parameters need to be identified and utilized to minimize these types of defects.

When examining the fracture behavior in the bending test, the fracture mechanism was observed and seen in Fig. 22. The bending process starts with the contact of the bending tool on the upper surface, and during bending, a crack forms on the welding surface to the left of the welding direction. This crack progresses diagonally towards the welding bottom surface, approaching the welding axis, causing fractures and failures in the internal structure of the specimen. The specimen withstands the bending force for a certain period, but ultimately loses its bending strength due to these fractures occurring within its internal structure.

In addition to the FSW data reported in the literature, the efficiency of weld seams produced by gas tungsten arc welding using tungsten electrode is also provided in the table. The absence of heat treatment in both materials has positively influenced the welding efficiency. The absence of heat treatment, along with the melting temperature, has reduced the decrease in strength. Due to the high weldability of the 5754-aluminum alloy, higher efficiency has been achieved compared to the other alloys.

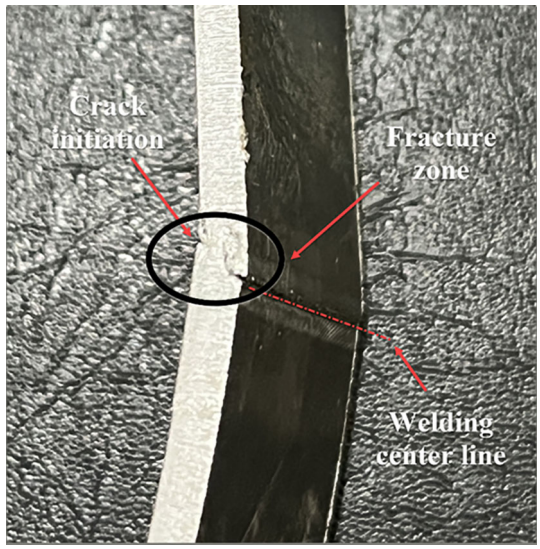

Fig. 22 Fractured specimen in the bending test

In the conducted experimental studies, a maximum efficiency of 54% was achieved. The reason behind this low welding efficiency is believed to be the use of inappropriate process parameters for the materials. Further research is definitely needed in this field. Increasing the number of parameters is necessary to determine the optimal ranges. Additionally, changes in the microstructure should be examined and evaluated. It is known that alloys with different properties exhibit different characteristics with temperature variations, which affect the efficiency. Due to the experiments being conducted on a CNC milling machine, the thrust force during plunging and the axial forces during advancement could not be measured. It would be more appropriate to conduct the experiments on specially designed machines for the FSW. This would enable better control over the parameters that need to be monitored during the process, resulting in more efficient welding with measurable values. To maintain the toughness of the welding base plate under heat and prevent thermal distortions, it is recommended to manufacture the base plate using hot work tool steels, which would prevent dimensional instability.

4. Conclusion

This investigation concludes that the FSW is a viable method for joining AA5754 and AA2024 aluminum alloys, provided that suitable parameters are chosen. Results reveal that the optimal parameters, specifically a rotational speed of 1200 rpm and a traverse speed of 45 mm/min, significantly enhance the weldability and mechanical properties of the joints. These parameters led to a welding efficiency of 54% for AA5754, 26% for AA2024, and 47% when combining these two alloys. The study highlighted that precise parameter settings are essential to minimize common defects such as void formation and enhance the mechanical integrity of the weld. Additionally, the research suggests that careful alignment of the material properties with welding parameters can lead to improved outcomes in the FSW, particularly when dealing with dissimilar materials. This study provides a clear direction for

future research and application in optimizing the FSW for various industrial applications involving aluminum alloys.

Funding

This work was supported by Kırşehir Ahi Evran University Scientific Research Projects Coordination Unit. Project Number: MMF.A4.22.008. Authors have greatly acknowledged the Kırşehir Ahi Evran University support.

Conflict of interest

The authors declare no conflict of interest.

References

1. W.M. Thomas, Friction Stir Butt Welding, in *International Patent Application* PCT/GB92/02203, 1991
2. X. Meng, Y. Huang, J. Cao, J. Shen and J.F. dos Santos, Recent Progress on Control Strategies for Inherent Issues in Friction Stir Welding, *Prog. Mater. Sci.*, 2021, **115**, 100706. https://doi.org/10.1016/j.pmatsci.2020.100706
3. X. Meng, Y. Xie, S. Sun, X. Ma, L. Wan, J. Cao and Y. Huang, Lightweight Design: Friction-Based Welding Between Metal and Polymer, *Acta Metallurgica Sinica (English Letters)*, 2023, **36**(6), p 881–898. https://doi.org/10.1007/s40195-023-01552-5
4. K. Kavathia and V. Badheka, Application of Friction Stir Welding (FSW) in Automotive and Electric Vehicle, *Recent Advances in Mechanical Infrastructure*. Springer Nature Singapore, Singapore, 2022, p 289–304
5. S. Shah, S. Tosunoglu, Friction Stir Welding: Current State of the Art and Future Prospects. in *16th World Multi-conference on Systemics, Cybernetics and Informatics*, Orlando, Florida, pp. 17-20 (2012)
6. T. Prater, Friction Stir Welding of Metal Matrix Composites for use in Aerospace Structures, *Acta Astronaut.*, 2014, **93**, p 366–373. https://doi.org/10.1016/j.actaastro.2013.07.023
7. M.M.Z. Ahmed, M.M. El-Sayed Seleman, K. Touileb, I. Albaijan, M.I.A. Habba, Microstructure, Crystallographic Texture, and Mechanical Properties of Friction Stir Welded Mild Steel for Shipbuilding Applications. Materials **15**(8), 2905 (2022)
8. S. Patnaik, S. Chattopadhyaya, S. Shankar, Friction Stir Welding and its Applications: an Overview. in *AIP Conference Proceedings* (2022)
9. S. Kilic, F. Ozturk and M.F. Demirdogen, A Comprehensive Literature Review on Friction Stir Welding: Process Parameters, Joint Integrity, and Mechanical Properties, *J. Eng. Res.*, 2023 https://doi.org/10.1016/j.jer.2023.09.005
10. S.W. Kallee, 5—Industrial Applications of Friction Stir Welding, in *Friction Stir Welding*, ed by D. Lohwasser, Z. Chen (Woodhead Publishing, Sawston, 2010). pp. 118-163
11. M. Enomoto, Friction Stir Welding: Research and Industrial Applications, *Weld. int.*, 2003, **17**(5), p 341–345
12. N. Bhardwaj, R.G. Narayanan, U. Dixit and M. Hashmi, Recent Developments in Friction Stir Welding and Resulting Industrial Practices, *Adv. Mat. Process. Technol.*, 2019, **5**(3), p 461–496
13. A. Wright, T.R. Munro and Y. Hovanski, Evaluating Temperature Control in Friction Stir Welding for Industrial Applications, *J. Manuf. Mater. Process.*, 2021, **5**(4), p 124
14. A. Grimm, S. Schulze, A. Silva, G. Göbel, J. Standfuss, B. Brenner, E. Beyer and U. Füssel, Friction Stir Welding of Light Metals for Industrial Applications, *Mater. Today: Proc.*, 2015, **2**, p S169–S178
15. B.T. Gibson, D.H. Lammlein, T.J. Prater, W.R. Longhurst, C.D. Cox, M.C. Ballun, K.J. Dharmaraj, G.E. Cook and A.M. Strauss, Friction Stir Welding: Process, Automation, and Control, *J. Manuf. Process.*, 2014, **16**(1), p 56–73. https://doi.org/10.1016/j.jmapro.2013.04.002
16. M. Guan, Y. Wang, Y. Huang, X. Liu, X. Meng, Y. Xie and J. Li, Non-weld-Thinning Friction Stir Welding, *Mater. Lett.*, 2019, **255**, 126506. https://doi.org/10.1016/j.matlet.2019.126506
17. X. Ma, Y. Xie, X. Meng, H. Chen, F. Wang, Y. Jiang, L. Wan and Y. Huang, Stepped-Shoulder Friction Stir Welding to Alleviate Weld Thinning for Dissimilar AA2195-T8/AA2219-T6 Alloys, *Sci. Technol. Weld. Join.*, 2021, **26**(8), p 599–605. https://doi.org/10.1080/13621718.2021.1982341
18. X. Ma, X. Meng, Y. Xie, Y. Zhao, X. Peng, M. Liang, D. Mao, L. Wan and Y. Huang, Elimination of Root Kissing Bond in Friction Stir Welding of Thick Plates, *Mater. Lett.*, 2022, **328**, 133148. https://doi.org/10.1016/j.matlet.2022.133148
19. T. Ding, H.-G. Yan, J.-H. Chen, W.-J. Xia and B. Su, Effect of Welding Speed on Microstructure and Mechanical Properties of Al−Mg−Mn−Zr−Tialloy Sheet During Friction Stir Welding, *Trans. Nonferrous Met. Soc. China*, 2021, **31**(12), p 3626–3642. https://doi.org/10.1016/S1003-6326(21)65753-9
20. M. Mahany, R.R. Abbas, M. Ahmed and H. Abdelkader, Influence of Tool Rotational Speed and Axial Load in Friction Stir Welding (FSW) of High Strength Alüminium Alloys, *Int. J. Res. Eng. Technol.*, 2017, **6**(02), p 114–120
21. H. Su, C.S. Wu, A. Pittner and M. Rethmeier, Simultaneous Measurement of Tool Torque, Traverse Force and Axial Force in Friction Stir Welding, *J. Manuf. Process.*, 2013, **15**(4), p 495–500. https://doi.org/10.1016/j.jmapro.2013.09.001
22. G.D.Q. Caetano, C.C. Silva, M.F. Motta, H.C. Miranda, J.P. Farias, L.A. Bergmann and J.F. dos Santos, Influence of Rotation Speed and Axial Force on the Friction Stir Welding of AISI 410S Ferritic Stainless Steel, *J. Mat. Process. Technol.*, 2018, **262**, p 430–436. https://doi.org/10.1016/j.jmatprotec.2018.07.018
23. B. Abnar, S. Gashtiazar and M. Javidani, Friction Stir Welding Of Non-Heat Treatable Al Alloys: Challenges and Improvements Opportunities, *Crystals*, 2023, **13**(4), p 576
24. G. Elatharasan and V.S.S. Kumar, An Experimental Analysis and Optimization of Process Parameter on Friction Stir Welding of AA 6061–T6 Aluminum Alloy using RSM, *Procedia Eng.*, 2013, **64**, p 1227–1234. https://doi.org/10.1016/j.proeng.2013.09.202
25. A. Lakshminarayanan and V. Balasubramanian, Process Parameters Optimization for Friction Stir Welding of RDE-40 Aluminium Alloy Using Taguchi Technique, *Trans. Nonferrous Met. Soc. China*, 2008, **18**(3), p 548–554
26. K. Praneetha, M. Apoorva, T. Prasanna Laxmi, S. Ravi Sekhar and S. Sravan Sashank, Experimental Investigation on Aluminium Alloy AA6082 and AA2014 Using the Friction Stir Welding, *Mater. Today Proc.*, 2022, **62**, p 3397–3404. https://doi.org/10.1016/j.matpr.2022.04.270
27. Y. Sun, D. He, F. Xue and R. Lai, Effect of Tool Rotational Speeds on the Microstructure and Mechanical Properties of a Dissimilar Friction-Stir-Welded CuCrZr/CuNiCrSi Butt Joint, *Metals*, 2018, **8**(7), p 526
28. Y. Zhao, J. Han, J.P. Domblesky, Z. Yang, Z. Li and X. Liu, Investigation of Void Formation in Friction Stir Welding of 7N01 Aluminum Alloy, *J. Manuf. Process.*, 2019, **37**, p 139–149. https://doi.org/10.1016/j.jmapro.2018.11.019
29. C. Meengam and K. Sillapasa, Evaluation of Optimization Parameters of Semi-solid Metal 6063 Aluminum Alloy from Friction Stir Welding Process Using Factorial Design Analysis, *J. Manuf. Mater. Process.*, 2020, **4**(4), p 123
30. S. Tiwari, D. Shukla and R. Chandra, Effect of Tool Tilt on Formation of Tunnel in Friction Stir Welded 5083 Joints: An Experimental Study, *J. Mater. Metall. Eng.*, 1991, **4**(2), p 10–15
31. A. Tamadon, A. Baghestani and M.E. Bajgholi, Influence of WC-Based Pin Tool Profile on Microstructure and Mechanical Properties of AA1100 FSW Welds, *Technologies*, 2020, **8**(2), p 34
32. M. Grujicic, G. Arakere, H. Yalavarthy, T. He, C.-F. Yen and B. Cheeseman, Modeling of AA5083 Material-microstructure Evolution During Butt Friction-stir Welding, *J. Mater. Eng. Perform.*, 2010, **19**, p 672–684
33. Y. Zhao, L. Zhou, Q. Wang, K. Yan and J. Zou, Defects and Tensile Properties of 6013 Aluminum Alloy T-Joints by Friction Stir Welding, *Mater. Des.*, 2014, **57**, p 146–155
34. R. Crawford, G. Cook, A. Strauss, D. Hartman and M. Stremler, Experimental Defect Analysis and Force Prediction Simulation of High Weld Pitch Friction Stir Welding, *Sci. Technol. Weld. Join.*, 2006, **11**(6), p 657–665
35. M. Cabibbo, C. Paoletti, M. Simoncini, A. Forcellese, Formability and Grained Structure Refinement of Cold-Rolled Friction Stir Welded

AA5754 Sheet. in *IOP Conference Series: Materials Science and Engineering: IOP Publishing*, p. 012001 (2019)
36. J.S.-A. Marvene Fernandes, F. Ozturk and F. Jarrar, Effect of Cold Air Jet Cooling on Weld Quality in Friction Stir Welding of AA2024-T351, *Res. Dev. Mat. Sci.*, 2022, **16**(3), p 1843–1851
37. Z. Haiyan and K.P. Mehta, Effect of Materials Positioning on Dissimilar Modified Friction Stir Clinching Between Aluminum 5754-O and 2024–T3 Sheets, *Vacuum*, 2020, **178**, 109445. https://doi.org/10.1016/j.vacuum.2020.109445
38. H.M. Anil Kumar, V. Venakata Ramana and S.P. Shanmuganathan, Experimental Investigation of Mechanical Properties And Morphological Studies on Friction Stir Welded Aluminum 2024 Alloy, *Mater. Today Proc.*, 2018, **5**(1), p 700–708. https://doi.org/10.1016/j.matpr.2017.11.136
39. Z.L. Hu, X.S. Wang, Q. Pang, F. Huang, X.P. Qin and L. Hua, The Effect of Postprocessing on Tensile Property and Microstructure Evolution of Friction Stir Welding Aluminum Alloy Joint, *Mater Charact*, 2015, **99**, p 180–187. https://doi.org/10.1016/j.matchar.2014.11.015
40. S. Memon, M. Paidar, S. Mehrez, K. Cooke, O.O. Ojo and H.M. Lankarani, Effects of Materials Positioning and Tool Rotational Speed on Metallurgical and Mechanical Properties of Dissimilar Modified Friction Stir Clinching of AA5754-O and AA2024-T3 Sheets, *Results Phys.*, 2021, **22**, 103962. https://doi.org/10.1016/j.rinp.2021.103962
41. D.E. GmbH (2023), Available from: https://www.doerrenberg.de/en/special-steels-en/. Accessed 09 April 2023
42. P. Sadeesh, M. Venkatesh Kannan, V. Rajkumar, P. Avinash, N. Arivazhagan, K. Devendranath Ramkumar and S. Narayanan, Studies on Friction Stir Welding of AA 2024 and AA 6061 Dissimilar Metals, *Procedia Eng.*, 2014, **75**, p 145–149. https://doi.org/10.1016/j.proeng.2013.11.031
43. Y. Xie, X. Meng, F. Wang, Y. Jiang, X. Ma, L. Wan and Y. Huang, Insight on Corrosion Behavior of Friction Stir Welded AA2219/AA2195 Joints in Astronautical Engineering, *Corros. Sci.*, 2021, **192**, 109800. https://doi.org/10.1016/j.corsci.2021.109800
44. V. Patel, W. Li, G. Wang, F. Wang, A. Vairis and P. Niu, Friction Stir Welding of Dissimilar Aluminum Alloy Combinations: State-of-the-Art, *Metals*, 2019, **9**(3), p 270
45. M.P. Iqbal, R. Jain and S.K. Pal, Numerical and Experimental Study on Friction Stir Welding of Aluminum Alloy Pipe, *J. Mater. Process. Technol.*, 2019, **274**, p 116–258
46. S. Verma and J. Misra, Study on Temperature Distribution During Friction Stir Welding of 6082 Aluminum Alloy, *Mater. Today Proc.*, 2017, **4**(2), p 1350–1356
47. Z. Ma, A. Feng, D. Chen and J. Shen, Recent Advances in Friction Stir Welding/Processing Of Aluminum Alloys: Microstructural Evolution and Mechanical Properties, *Crit. Rev. Solid State Mater. Sci.*, 2018, **43**(4), p 269–333
48. J. Li, M. Su, W. Qi, C. Wang, P. Zhao, F. Ni and K. Liu, Mechanical Property and Characterization of 7A04-T6 Aluminum Alloys Bonded by Friction Stir Welding, *J. Manuf. Proces.*, 2020, **52**, p 263–269
49. Q. Wen, W. Li, V. Patel, Y. Gao and A. Vairis, nvestigation on the Effects of Welding Speed on Bobbin Tool Friction Stir Welding of 2219 Aluminum AlloyI, *Met. Mater. Int.*, 2020, **26**, p 1830–1840
50. O. Doktaş, Sürtünme Karıştırma Kaynağının Farklı Kalınlıktaki Alüminyum Parçalara Uygulanması, master's thesis, Istanbul Aydin University (2019)
51. E.Y. Keskin, Investigation of weld quality for friction stir welding of extruded 6000 series aluminum alloys, master's thesis, Turkish—German University (2019)
52. S. Çelik and F. Tolun, Effect of Double-sided Friction Stir Welding on the Mechanical and Microstructural Characteristics of AA5754 Aluminium Alloy, *Mater. Test.*, 2021, **63**(9), p 829–835. https://doi.org/10.1515/mt-2021-0009
53. M.P. Iqbal, R.K. Vishwakarma, S.K. Pal and P. Mandal, Influence of Plunge Depth During Friction Stir Welding of Aluminum Pipes, *Proc. Inst. Mech. Eng. Part B*, 2020 https://doi.org/10.1177/0954405420949754
54. H.M. Jamalian, M. Farahani, M.B. Givi and M.A. Vafaei, Study on the Effects of Friction Stir Welding Process Parameters on the Microstructure and Mechanical Properties of 5086–H34 Aluminum Welded Joints, *Int. J. Adv. Manuf. Technol.*, 2016, **83**(1–4), p 611–621
55. D. Kumar Rajak, D.D. Pagar, P.L. Menezes and A. Eyvazian, Friction-based Welding Processes: Friction Welding and Friction Stir Welding, *J. Adhes. Sci. Technol.*, 2020, **34**(24), p 2613–2637
56. E.H. Türkyılmaz, Sürtünme karıştırma kaynağı birleştirmelerinde farklı karıştırma uç formlarının bileştirme esnasında oluşturduğu kuvvetlerin deneysel incelenmesi, Yüksek Lisans Tezi, Gazi Üniversitesi (2019)
57. V. Msomi and N. Mbana, Mechanical Properties of Friction Stir Welded AA1050-H14 and AA5083-H111 Joint: Sampling Aspect, *Metals*, 2020, **10**(2), p 214
58. Y. Huang, X. Meng, Z. Lv, T. Huang, Y. Zhang, J. Cao, L. Zhou and J. Feng, Microstructures and Mechanical Properties of Micro Friction Stir Welding (μFSW) of 6061–T4 Aluminum Alloy, *J. Mater. Res. Technol.*, 2019, **8**(1), p 1084–1091
59. S. Shanavas and N. Murugan, Weldability of Marine Grade AA 5052 Aluminum Alloy by Underwater Friction Stir Welding, *Int. J. Adv. Manuf. Technol.*, 2018, **95**(9–12), p 4535–4546
60. S. Fouladi, A.H. Ghasemi, M. Abbasi, M. Abedini, A.M. Khorasani and I. Gibson, The Effect of Vibration During Friction Stir Welding on Corrosion Behavior, Mechanical Properties, and Machining Characteristics of Stir Zone, *Metals*, 2017, **7**(10), p 421
61. M. Bevilacqua, F.E. Ciarapica, A. D'Orazio, A. Forcellese and M. Simoncini, Sustainability Analysis of Friction Stir Welding of AA5754 Sheets, *Procedia CIRP*, 2017, **62**, p 529–534
62. P.N. Karakizis, D.I. Pantelis, D.A. Dragatogiannis, V.D. Bougiouri and C.A. Charitidis, Study of Friction Stir Butt Welding Between Thin Plates of AA5754 and Mild Steel for Automotive Applications, *Int. J. Adv. Manuf. Technol.*, 2019, **102**(9), p 3065–3076. https://doi.org/10.1007/s00170-019-03388-9
63. H. Mehdi and R. Mishra, Study of the Influence of Friction Stir Processing on Tungsten Inert Gas Welding of Different Aluminum Alloy, *SN Appl. Sci.*, 2019, **1**, p 1–11
64. N. Akçakale, Mechanical and Microstructural Properties of AL 5754 Alloy Joined by GMAW and GTAW, *J. Eng. Technol. App. Sci.*, 2021, **6**(1), p 23–36